Article

# Synthesis of Onion-Like δ-MoN Catalyst for Selective Hydrogenation

Shanmin Wang,[*,†,§,⊥,○] Hui Ge,[*,‡] Wenpeng Han,[‡] Yongjun Li,[∥] Jianzhong Zhang,[#] Xiaohui Yu,[¶] Jiaqian Qin,[▽] Zewei Quan,[†] Xiaodong Wen,[‡] Xuekuan Li,[‡] Liping Wang,[§] Luke L. Daemen,[○] Duanwei He,[⊥] and Yusheng Zhao[*,†,§]

[†]Southern University of Science & Technology of China, Shenzhen, Guangdong 518055, China

[‡]Institute of Coal Chemistry, Chinese Academy of Sciences, Taiyuan, Shanxi 030001, China

[§]HiPSEC & Physics Department, University of Nevada, Las Vegas, Nevada 89154, United States

[∥]Hubei Better Materials Co., Ltd., Hong'an, Hubei 438408, China

[⊥]Institute of Atomic & Molecular Physics, Sichuan University, Chengdu 610065, China

[#]Materials Science & Technology Division, Los Alamos National Laboratory, Los Alamos, New Mexico 87545, United States

[○]Oak Ridge National Laboratory, Oak Ridge, Tennessee 37831, United States

[¶]Institute of Physics, Chinese Academy of Sciences, Beijing, 100190, China

[▽]Metallurgy & Materials Science Research Institute, Chulalongkorn University, Bangkok, 10330, Thailand

Ⓢ Supporting Information

ABSTRACT: Synthesis of base metal catalysts with well-defined structure and morphology is highly desired to achieve high catalytic performance for clean energy and green chemistry applications. However, in most catalyst synthesis, it is challenging to control structural manipulation at the nanoscale, especially for transition-metal nitrides, because they are often thermodynamically unfavorable at atmospheric pressure. In this work, we report a high-pressure approach for the formation of hexagonal δ-MoN nanocrystals with a unique onion-like morphology. The onion layers are made of stacked zigzag Mo−N shells associated with the (101) crystallographic plane. Impressively, the as-synthesized δ-MoN possesses intrinsic catalytic activities that are twice

higher than the traditional MoS₂ for hydrodesulfurization of dibenzothiophene and more than five times higher in the selectivity to hydrogenation. The nitride is also highly active for selective hydrogenation of diverse nitroarenes to anilines at mild conditions. The enhanced catalytic properties are presumably attributed to the unique zigzag Mo−N bonding structure of the nitride. This work demonstrates that high-pressure synthesis is a viable approach to design and fabricate new and cost-effective transition-metal nitride catalysts for diverse hydrogenation applications.
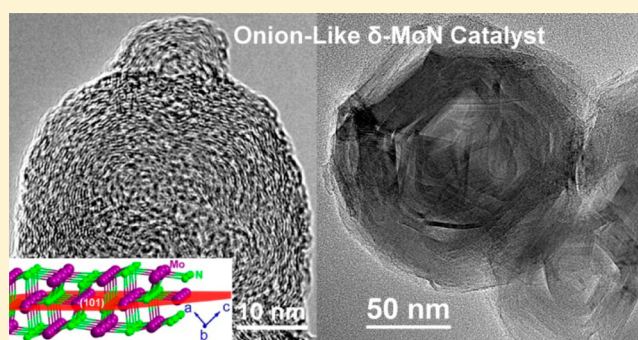
■ INTRODUCTION

Heterogeneous catalysis is a common strategy used in a chemical reaction for rate acceleration and product selectivity, and advancement in this field plays a key role in today's world for achieving more sustainable and greener chemistry.[1−3] Owing to high thermal stability, ease of recovery, and reuse,[4,5] heterogeneous catalysts have widely been studied and exploited for industrial synthesis of a broad range of chemicals and petrochemicals.[1,2] Development of new catalysts, preferably made from inexpensive earth-abundant elements with high activity and selectivity, are highly demanded for more energy and cost-effective solutions. In principle, catalytic properties of a material completely depend on the underlying electronic structure.[6,7] Manipulation of a material's composition and structure, and hence the electronic structure, provides many opportunities for fabricating new catalysts. For materials

at the nanoscale, the structural manipulation also includes geometric shape and surface morphology. Compared to compositional manipulation, structural manipulation sometime involves special synthetic procedures, such as colloidal,[8] co-precipitation,[9] and electrodeposition methods.[10] Nevertheless, a number of recent studies along this direction have led to the discovery of new catalysts with well-defined, diverse geometrical features as reviewed most recently in refs 3, 11, and 12. It is worth noting that most of the such-produced catalysts involve precious metals, which would present a remarkable barrier against their commercial viability.[13,14]

In the traditional design of catalytic materials, the MoS_2-based catalysts represent one of extraordinarily successful stories,[1] and have extensively been used for many applications,[1,15−17] mainly due to its layered structure with loosely bonded interlayers. This structural virtue substantially facilitates production of a variety of nano-clusters with sufficiently exposed active sites on the surfaces of the S−Mo−S sandwich slabs. The success in MoS_2-based catalysts largely relies on the effective exposure of catalytically more favorable edges.[18,19] For heterogeneous catalysts, it has long been recognized that their catalytic properties are closely tied to the surface atomic arrangement. As a typical example, the platinum (111) facet is catalytically more active than the (100) plane for a number of processes, such as dehydrogenation of cyclohexene[20] and oxygen reduction reaction.[21] However, for most material systems due to a lack of layered structure, it is a non-trivial task to experimentally synthesize a catalyst with desired crystal geometry and sufficiently exposed yet catalytically active surfaces at the nanoscale. This is because the associated surface may correspond to a high-index facet and is often thermodynamically unstable. As a result, despite several decades of experimental efforts, some industrially important processes are still limited to a few classes of catalysts. The MoS_2-based compounds, for example, prevail the catalyst market for the hydroprocessing of transportation fuels.[1] Clearly, it calls for entirely new catalysts to ultimately enhance the catalytic performance.

Interestingly, recent advances in nitrogen-doped A_xO (A = Fe and Co) catalysts suggest that their superior catalytic properties for selective hydrogenation processes are intimately linked to the nitrogen atoms,[4,22] in the sense that the incorporated nitrogen atoms introduce unique adsorption modes with more selectivity of special group.[4,22] From this point of view, the nitrogen atom is catalytically more active and may work synergistically with transition metal for precious catalysis processes. In fact, transition-metal (TM) nitrides have recently attracted considerable interest because they exhibit a number of useful catalytic properties for hydrotreating (e.g.,W_2N),[23−25] hydrogenolysis (e.g., Mo_2N),[26] photochemistry (e.g., Ta_3N_5),[27] and electrochemistry (e.g., Mo_2N),[28,29] in spite of the fact that none of them has well-defined, catalytically favored geometries. In addition, TM nitrides are often intrinsically resistant to corrosion, oxidation, or decomposition; thus, they can be used in harsh reaction environments, such as sour catalysis.[30] Among them, hexagonal molybdenum mononitride, δ-MoN, represents one of more promising catalysts as it has shown similar catalytic activities as platinum-group catalysts.[28,31] However, for most TM nitrides, it is difficult to tailor their catalytic properties by structural manipulation, because formation of TM nitrides is often thermodynamically unfavorable at atmospheric pressure. As a result, TM nitrides as a group, including δ-MoN, are relatively less explored for their catalytic performance in different applications.

Over the past decade, a surge of new TM nitrides have successfully been synthesized in the Zr−N,[32,33] Hf−N,[32] Ta−N,[34,35] and noble metal nitride systems at high pressure.[36−39] These findings demonstrate that pressure can effectively promote the involvement of d-electrons in chemical bonding with nitrogen and hence the formation of nitrides of higher oxidation states for the constituent metals.[40] Using the newly formulated high-P ion-exchange reactions,[41,42] we have recently synthesized a number of novel nitrides (such as W_2N_3, W_3N_4,

and $3R$-MoN_2)[30,40] at moderate pressures up to 5 GPa. In particular, the newly discovered $3R$-MoN_2 with a layered structure exhibits a series of attractive properties.[30,43,44] Intriguingly, the crystal morphology and geometry of TM nitrides (e.g., VN and MoN)[45,46] can be readily tuned by the control of synthetic temperature, reaction time, or sample environment, which offers great opportunities for the formation of nitride crystals with new structural morphologies bearing superior catalytic performances. In this work, we extended this high-pressure synthesis protocol to δ-MoN and have successfully synthesized onion-like nanocrystals with each layer composed of a puckered and bent (101) crystalline sheet. The catalytic properties of the as-synthesized sample were further evaluated for selective hydrogenation processes.

■ EXPERIMENTAL SECTION

High-Pressure Synthesis and Purification. Anhydrous sodium molybdate (Na_2MoO_4) (>99.5%, ∼ 50 μm) and hexagonal boron nitride (hBN) (>99.9%, ∼ 50 μm) powders were used as starting reactants. Anhydrous sodium molybdate was obtained by dehydration of commercially available $Na_2MoO_4 \cdot 2H_2O$ in a muffle furnace at 473 K for 12 h. To improve the grain size distribution of the final reaction product, the starting materials in the molar ratio Na_2MoO_4:BN = 1:2 were homogeneously mixed to enable a widespread nucleation and growth of crystals.

High-pressure (P) synthesis was performed in a cubic DS 6 × 14 MN high-P apparatus at Sichuan University and a DS 6 × 40 MN cubic press at Hubei Better Materials Co., Ltd., China.[47] In each experiment, the powder mixture was compacted into a cylindrical pellet of 12−25 mm diameter and 5−10 mm length, which was then sealed in a molybdenum capsule to prevent possible contamination. At a target pressure between 3 and 5 GPa, the sample was gradually heated to a desired temperature (T) in the 973−1773 K range and soaked for 10−25 min before quenching to room temperature and subsequent decompression to ambient pressure. The crystallite size of the run product was controlled by reaction temperature and reaction time. The detailed experimental procedures have been described elsewhere.[30,47] To obtain phase-pure sample, the run products were washed with distilled water to remove the byproduct $NaBO_2$, followed by drying in an oven at 348 K.

Characterization. The final products were characterized by X-ray diffraction (XRD) with Cu Kα radiation and time-of-flight neutron diffraction at the HiPPO flightpath of Los Alamos Neutron Science Center (LANSCE), Los Alamos National Laboratory. The crystal structure was determined from Rietveld refinement of the X-ray and neutron diffraction data using the GSAS program. Microstructures of the purified sample were characterized by high-resolution transmission electron microscopy (HRTEM).

To study phase stabilities of as-synthesized nitride, thermogravimetric mass spectrometer (TG−MS) measurements were carried out in an Ar atmosphere on a Setaram TGA-92 instrument equipped with an OmniStar-200 quadrupole mass spectrometer. A simultaneous TG−DTG (derivative thermogravimetry) measurement was performed in air to study oxidation of the nitride. For each experimental run, phase-pure nitride powders (∼10 mg) were loaded and heated to a target temperature of 1273 K at a rate of 10 K·min^{-1}. The nitrogen content, x, in the obtained MoN_x, was determined from oxidation-induced mass change based on TGA−DTG measurement in air.[30,40]

The specific surface area and pore structures of the nitride catalyst were determined from physisorption of N_2 by using the BET and BJH methods at 77 K and low relative pressure (P/P_0) of 0–0.3, where P and P_0 are the equilibrium pressure and saturation pressure of N_2, respectively.[48] The measurement was performed in a Tristar-3000 instrument. Traditional MoS_2 catalyst was also measured for comparison. Prior to measurement, each of the two catalysts was thermally treated at 473 K in a vacuum for 6–8 h to remove possible impurity gases adsorbed on the powder particles.

The temperature-programmed desorption (TPD) measurement of the pre-adsorbed NO gas was conducted in a TP-5080 quartz microreactor to determine the concentration of active Mo atoms in the catalysts. To remove possible adsorbed impurity gases, the samples (~100 mg) were treated at 623 K for 30 min in a He atmosphere with a flow rate of 30 mL·min⁻¹, followed by cooling the sample to 323 K over a period of 60 min. Prior to desorption, chemisorption of NO was carried out at 323 K in a He atmosphere with a 0.4% volume fraction of NO. The mixed gases of NO and He were flowed for 60 min at a flow rate of 50 mL·min⁻¹ to optimize adsorption efficiency. In order to eliminate the physisorbed NO, the catalyst was then flushed in a He flow at 323 K for 60 min with a flow rate of 30 mL·min⁻¹. The subsequent desorption process of NO was monitored at temperatures up to 673 K with a heating rate of 10 K·min⁻¹. In all these processes, the volume of the desorbed NO was determined by a quadrupole mass spectrometer, OmniStar GSD-320, which was pre-calibrated by using standard mixed gases of He and NO and the calibrated parameter is ~13.147 mol of NO per unit area.

Catalytic Properties. The catalytic hydrodesulfurization (HDS) of dibenzothiophene (DBT) using δ-MoN and MoS_2 catalysts was carried out in a high-P batch reactor/autoclave at 623 K and 6 MPa in a H_2 atmosphere. Before the experiment, 500 ppm DBT was dissolved as feedstock into 90.0 g of decalin (or 101.1 mL in volume). For each experimental run, 0.3 g catalyst was placed in the reactor with a stirring speed of 300 rpm. At 623 K, the reaction product was sampled every 8 h for a total of 48 h. To further verify catalyst stability, the phase of recovered catalyst was checked by X-ray diffraction measurement (see Supporting Information, Figure S6), indicating that no phase change occurred during catalytic reaction.

The selective hydrogenation of functionalized nitro compounds (i.e., substrates) was carried out in a 50 mL autoclave reactor using the as-synthesized δ-MoN catalyst. Before each catalysis reaction, a target substrate of 1.675 mmol was dissolved into a 20 mL isopropyl alcohol with 0.2 g decalin (i.e., $C_{10}H_{18}$) as internal standard for quantitatively determining the concentration of final product. The δ-MoN catalyst powders (0.405 mmol) and hydrazine hydrate (i.e., $N_2H_4\cdot H_2O$), a reducing agent, were then added into the mixed reactant medium. The molar ratios between substrate and $N_2H_4\cdot H_2O$ are typically 1:3 or 1:4 to provide sufficient terminal reductant for the catalytic reaction. Such-prepared reaction mixture was then sealed in a nitrogen atmosphere of 1 MPa and heated with stirring to a target reaction temperature in the 373–393 K range for 8–24 h. To analyze the final reaction products, the catalyst was centrifugally separated, leaving behind a solution mixture only containing the reaction product, which was qualitatively analyzed in a gas chromatograph–mass spectrometer, Shimadzu GC–MS 2010. To obtain quantitative analysis, a flame ionization detector, FID, was employed on the Shimadzu GC-2010 (see Supporting Information, Figure S7).

■ RESULTS AND DISCUSSION

Figure 1a shows an X-ray diffraction (XRD) pattern of the final product, which was purified from high $P–T$ synthesis at 4 GPa
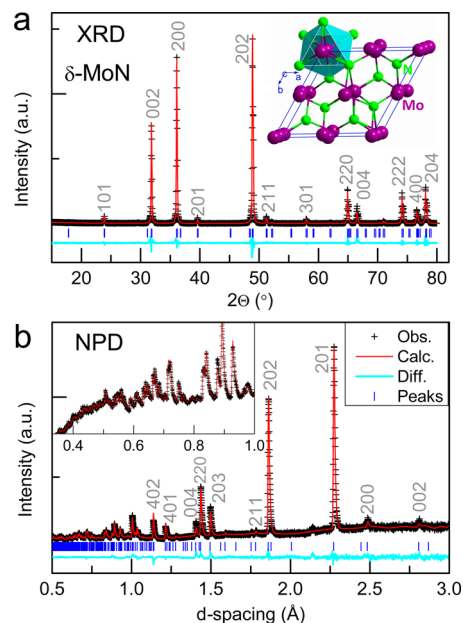

Figure 1. Refined XRD and NPD patterns of hexagonal δ-MoN synthesized at 4 GPa and 1773 K for 10 min. (a) XRD data collected with Cu $K\alpha_{1,2}$ radiation. Inset is a polyhedral view of crystal structure. (b) NPD data collected at scattering angle of 144°. Both XRD and NPD data were taken at ambient conditions.

and 1773 K for 10 min. Apparently, the recovered sample is phase-pure, and all Bragg reflections can be indexed by a hexagonal unit cell with space group $P6_3mc$ (No. 186), which is commonly referred to as δ_3-MoN, one of the polymorphs of hexagonal MoN,[49] and is thereafter denoted as δ-MoN for simplicity. The other two hexagonal polymorphs, δ_1 and δ_2, are metastable low-T phases adopting slightly different structures, WC-type ($P\bar{6}m2$, No. 187) for δ_1 and NiAs-type ($P6_3/mmc$, No. 194) for δ_2, mainly due to the ordering of nitrogen atoms along the c-axis in the latter phase.[49,50] In contrast, the Mo atoms in δ-MoN tend to form a unique trigonal cluster, and its crystal structure can be viewed as a slightly deformed $2 \times 2 \times 1$ superstructure of δ_2 phase.[49] Interestingly, for well-crystallized δ-MoN, the unit cell tends to expand along a-axis;[42,44] concurrently, the lattice contracts along c-axis.[49,51] This unusual phenomenon can be understood in terms of the disordering of Mo and ordering of N atoms along a- and c-axis, respectively. Compared with reported values (i.e., $a = 5.735$ Å and $c = 5.6281$ Å),[49] the high-P synthesized sample with larger $a = 5.7417$ (5) Å and smaller $c = 5.6187$ (3) Å (see Figure 1a) indicates improved crystallinity.

To further investigate the crystal structure, a neutron powder diffraction (NPD) measurement was conducted on the purified run product. At the first glance, the NPD pattern of Figure 1b appears to be quite different from the XRD pattern. Remarkably, the strongest Bragg reflection from NPD, the (201) plane, is almost extinct in the XRD measurement (Figure 1a). This is because the N atom scatters neutrons very well with a coherent scattering length of ~9.36 fm, which is ~40% larger than that of Mo (~6.72 fm).[52] By contrast, the diffraction intensity in XRD is dominated by scattering from Mo atoms.

Therefore, when NPD is combined with XRD, the atomic positions for both Mo and N can be accurately determined from Rietveld analysis. Details of the refined crystal structure of as-synthesized δ-MoN are listed in Table 1 (also see Supporting Information, Figure S1).

Table 1. Refined Lattice Parameters for High-*P* Synthesized δ-MoN

	hexagonal δ-MoN
cell content	Mo_8N_8
space group	*P6₃mc* (No. 186)
experimental conditions	ambient conditions
lattice parameter *a*, *c* [Å]	5.7417 (5), 5.6187 (3)
Mo sites (XRD)	Mo1: *6c* (*x*, −*x*, *z*) (*x* = 0.4877, *z* = 0)
	Mo2: *2a* (0, 0, *z*) (*z* = 0)
N sites (XRD)	N1: *6c* (*x*, −*x*, *z*) (*x* = 0.8285, *z* = 0.1734)
	N2: *2b* ($^1/_3$, $^2/_3$, *z*) (*z* = 0.2153)
N sites (NPD)	N1: *6c* (*x*, −*x*, *z*) (*x* = 0.8302, *z* = 0.2438)
	N2: *2b* ($^1/_3$, $^2/_3$, *z*) (*z* = 0.2612)
cell volume [Å³]	160.419
density [g·cm⁻³]	9.105
d_{Mo-Mo} [Å]	2.660, 2.809−2.873
d_{Mo-N} [Å] (NPD)	2.12−2.23
R_p [%], χ^2	8.84, 2.27

It is worthwhile pointing out that the synthesis of δ-MoN is experimentally challenging, especially in the context of massive and industrial-scale production. For traditional reaction routes at atmospheric pressure, including chemical vapor deposition (CVD) or other deposition techniques[49,53,54] and ammonolysis or nitridation of Mo-bearing compounds,[49,51,55] the reported final products are mostly low-*T* phases (i.e., δ_1 or δ_2 phase) in the form of thin films on a milligram scale. Only a few processes allow preparation of δ-MoN$_x$ (i.e., δ_3 phase), because it is a high-*T* phase and often forms within a narrow temperature range of 953−1000 K.[49,53] Under high pressure, δ-MoN$_x$ has previously been synthesized by a number of methods such as high *P*−*T* sintering of low-*T* δ_1-MoN$_x$ phase,[47,52] nitridation of Mo_2N,[56] and reaction between NH₄Cl and MoO₂.[57] However, the final product is either limited to a small scale or accompanied by significant amount of impurity phases (e.g., unreacted metal Mo and MoO₂).[56,57] To obviate the afore-mentioned drawbacks, we have formulated a new high-*P* reaction route for the synthesis of δ-MoN, given by

$$Na_2MoO_4 + 2BN = MoN + 2NaBO_2 + {}^1/_2 N_2 \quad (1)$$
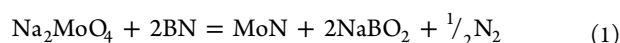
The reaction can be simply viewed as ion exchange between Mo^{6+} and $B^{3−}$. The byproduct NaBO₂ can readily be removed from the experimental run product by washing with water to obtain phase-pure nitride. Using the same route, we have discovered a new, nitrogen-rich 3R−MoN₂ at a relatively low temperature of 753 K.[30] Similarly, based on the ion-exchange concept of reaction 1, we have designed and obtained a number of other binary nitrides including W_2N_3,[40] CrN,[41,42,45] VN,[45] and GaN,[58,59] indicating that this methodology of nitride synthesis is likely suitable for variety of transition metals in the periodic table.

Figure 2 shows some typical high-resolution transmission electron microscopy (HRTEM) images for δ-MoN powders synthesized under high *P*−*T* conditions. Apparently, the crystals display a spherical shape in nanoscale, and the crystallite size distribution is statistically within a narrow range of 20−60 nm (see Figure 2a and Supporting Information, Figure S2). A very small fragment of the sample has crystallite size greater than 100 nm (Figure 2c), which may be attributed to the temperature gradient of high-*P* cell. On a closer inspection, each crystal in Figure 2b−d exhibits an intriguing pattern of loops and whorls resembling fingerprints (also see Supporting Information Figure S3), inferring that crystals have an onion-like morphology. On an atomic scale, the "onion" layers consist of concentrically stacked MoN spherical shells (Figure 2d). Contrary to what one might expect, such spherical shells correspond to the (101) crystallographic planes in the δ-MoN lattice, instead of the (002) planes, with a characteristic spacing of ∼3.7 Å (Figure 2d), close to the refined value of 3.7237 Å. Interestingly, for crystals with smaller gain size (i.e., below 60 nm), remarkable lattice disorder is observed in the (101) onion shells with abundant puckering and stacking faults as presented in Figure 2b and Figure S3, which is similar what has been reported for onion-like BN and MoS₂ (see refs 60 and 61 for HRTEM images). In larger crystals, the lattice disorder is drastically reduced as shown in Figure 2c,d. The deformation of the (101) crystal shells in the form of bending is clearly demonstrated on the atomic scale in Figure 2d, which leads to the concentrically assembled spherical lattice shells. According to the refined crystal structure, the Mo−N bonds in the (101) plane are organized with a large zigzag structure (Figure 2d and Supporting Information, Figure S3c). Although uncommon, nano-ribbons are sometimes observed (Figure 2e), which is composed of more than a dozen of (101) shells with distinct boundaries. In addition, the (112) and (200) fringe patterns can also be observed and identified as shown Figure 2e,f. As expected for a hexagonal structure, the selected HRTEM image in Figure 2g clearly shows hexagonally stacked Mo atoms on the exposed (200) facet. Also noted is that the crystallite size of δ-MoN powders can readily be tuned by the control of synthesis temperature and heating time. With increasing synthesis temperature at 5 GPa, the crystallite size increases from a few nanometers at 973 K to more than 30 nm at 1473 K for the same heating time of 15 min (see Supporting Information, Figure S4). Using the same high-*P* ion-exchange reaction and a prolonged heating process, the large plate-like single-crystal δ-MoN of 50 um can also been synthesized with well-defined (002) facets, further suggesting that the crystalline morphology of this nitride can be manipulated during high *P*−*T* synthesis.[46]

To the best of our knowledge, the onion-like structure is found merely in material systems with layered structures such as graphite,[62,63] g-CN$_x$,[64] BN,[60] and MoS₂.[61] In all these materials, the onion layers are loosely held together by the weak van der Waals forces. By contrast, the non-layered δ-MoN, although having a hexagonal structure, is one of the hardest, highly incompressible metal nitrides due to the strong Mo−N bonding network.[46] Because the low-index (002) and (001) planes are energetically more stable, they often occur predominantly on the exposed surface of hexagonal MoN crystals synthesized using traditional methods.[46,49,53,65] However, in δ-MoN crystals synthesized under high pressure, the exposed surface is typically associated with the high-index (101) plane. This structural characteristics may provide catalytically active sites because of a unique zigzag Mo−N bonding structure in the (101) plane. In contrast, the (002) plane is composed solely of Mo atoms (see Figure 1a and Figure 2g). As mentioned above, the exposure of nitrogen atoms on the crystal's surface can introduce adsorption modes
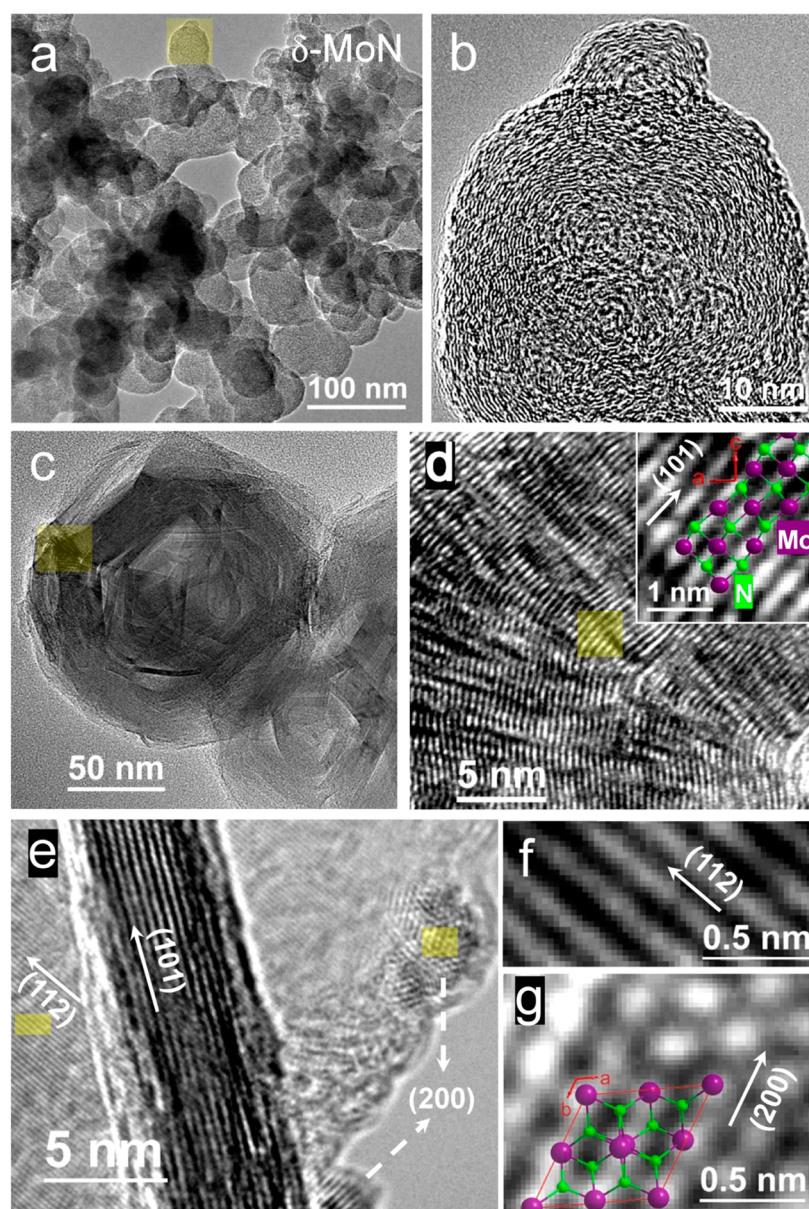
Figure 2. TEM images of purified δ-MoN. (a) Spherical nanoparticles of δ-MoN. (b, c) Onion-like morphology of δ-MoN nanoparticles. (d−g) HRTEM images with atomic-scale views of (101), (112), and (200) planes. Enlarged images b, d, f, and g correspond to the highlighted portions in images a, c, and e to show fingerprint detail. In the top-right corner of parts d, the inset is an enlargement of highlighted portion. In parts d and g, crystal structures of δ-MoN with preferred crystallographic orientations along the (101) and (200) planes are also added as insets. The white solid arrows in parts d−g denote the viewing direction for each family of crystal planes.

for some molecules,[4,22] giving rise to catalytic selectivity for some catalysis reactions.

As shown in Figure 3, thermal stabilities of the onion-like δ-MoN catalyst were determined by simultaneous thermogravimetry−derivative thermogravimetry (TG−DTG). In air, a remarkable weight increase was observed at ~673 K, which corresponds to the onset of oxidation of MoN, higher than the oxidation temperature of MoN_2 (~610 K) and MoS_2 (~623 K).[30] Evidently, the oxidation process is complete when a plateau value is reached at ~830 K, which is higher than that in 3R-MoN_2 (i.e., 780 K), and the final product is MoO_3.[30] From the thermogravimetric data, nitrogen concentration in the nitride is determined to be $x = 1.0(1)$ in MoN_x, further confirming the stoichiometry of the nitride. The similar method has been used for determining nitrogen content in W_2N_3 and

3R-MoN_2.[30,40] With further increase in temperature, the sublimation of MoO_3 happens at ~1000 K as the weight decreases steeply, close to reported temperature in 3R-MoN_2.[30] On the other hand, as temperature is elevated in an Ar atmosphere, there is no decomposition observed up to the highest experimental temperature of 1273 K, indicating that δ-MoN has an excellent stability and is more stable than CrN (i.e., stable only below 1073 K).[41]

To evaluate catalytic properties of onion-like δ-MoN, we performed hydrodesulfurization (HDS) measurement of dibenzothiophene (DBT), which is a common sulfur-bearing molecule in diesel fuels. As a standard catalyst, traditional MoS_2 was also tested for comparison purpose. In both cases, the catalysts are neither supported nor promoted to determine their intrinsic catalytic performance. To achieve an appropriate
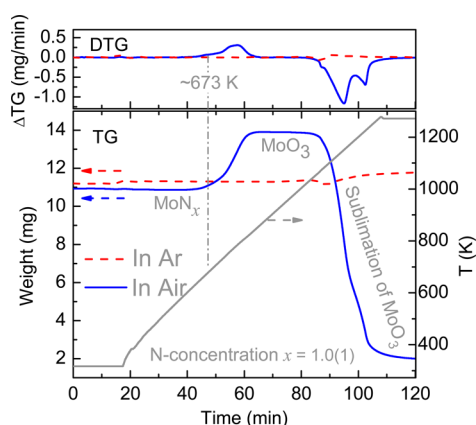
Figure 3. Thermogravimetry (TG) and differential thermal gravity (DTG) measurements of δ-MoN performed in air and argon. In air, the oxidation of δ-MoN occurs around 673 K and leads to a final product of MoO_3, which starts sublimating at ~1000 K. The derived nitrogen concentration, x, is close to 1.0 in MoN_x. In Ar, the nitride remains stable up to 1273 K, the highest experimental temperature.

evaluation, the surface area and pore structure of δ-MoN and MoS_2 catalysts were characterized by N_2 physisorption using the BET and BJH methods (see Experimental Section and ref 30). The thus-obtained data are summarized in Table 2. As

Table 2. Summary of NO Uptake Data, BET Surface Area, Pore Volume, and Pore Width for δ-MoN and MoS_2 Catalysts, with the Pseudo-First-Order Rate Constants, k, Also Listed, Normalized to the Active Mo Sites

catalyst	δ-MoN	MoS_2	ratio δ-MoN:MoS_2
BET surface area $[m^2 \cdot g_{cat}^{-1}]$	1.221	3.699	0.33
pore volume $[\mu \cdot m^3 \cdot g_{cat}^{-1}]$	0.004	0.016	0.25
ave. pore width [nm]	14.14	17.14	0.83
NO uptake $[\mu \cdot mol_{NO} \cdot g_{cat}^{-1}]$	18.04	46.31	0.39
NO/Mo $[\times 10^{-3} \, mol_{NO} \cdot mol_{Mo}^{-1}]^a$	1.984	7.414	0.27
k $[L_{Oil} \cdot mol_{NO}^{-1} \cdot s^{-1}]$	0.061	0.033	1.85

^{a}NO in the NO/Mo ratio denotes the molar volume of NO adsorbed onto the coordinately unsaturated Mo sites. The NO/Mo ratios represent the percentages of catalytically active Mo sites.

commonly accepted, the coordinately unsaturated Mo sites on the catalyst's surface are closely associated with catalytically active centers. In addition, the pore structure of the catalyst is equally important because, for a given catalyst, some pore-size distributions may be completely inaccessible for large reactant molecules, which would result in reduced rate of conversion to products.

As tabulated in Table 2, the determined specific surface area for δ-MoN is 1.221 $m^2 \cdot g_{cat}^{-1}$, which is only one-third of the value of MoS_2 catalyst (i.e., 3.699 $m^2 \cdot g_{cat}^{-1}$) and more than 1 order of magnitude smaller than that of commercial MoS_2-based catalysts.[66] Similar behaviors have also been found in the pore volume.[66] Thus, from the consideration of surface area and pore sizes the as-synthesized δ-MoN is extrinsically unfavorable for achieving high catalytic activity. In this work, we focus our investigation on the intrinsic properties of the catalysts by a comparative approach. For two catalysts with the comparable pore sizes (Table 2), the catalytic activity of δ-MoN can be normalized in term of specific surface area and, to a first approximation, assessed relative to the traditional MoS_2.

However, the activity of a catalyst largely relies on the concentration of catalytically active centers rather than surface area. We thus determined the concentration of active Mo sites for both catalysts, using chemisorption−desorption of NO molecules (i.e., the NO uptake measurement). As plotted in Figure 4a, the observed desorption spectra for the two catalysts
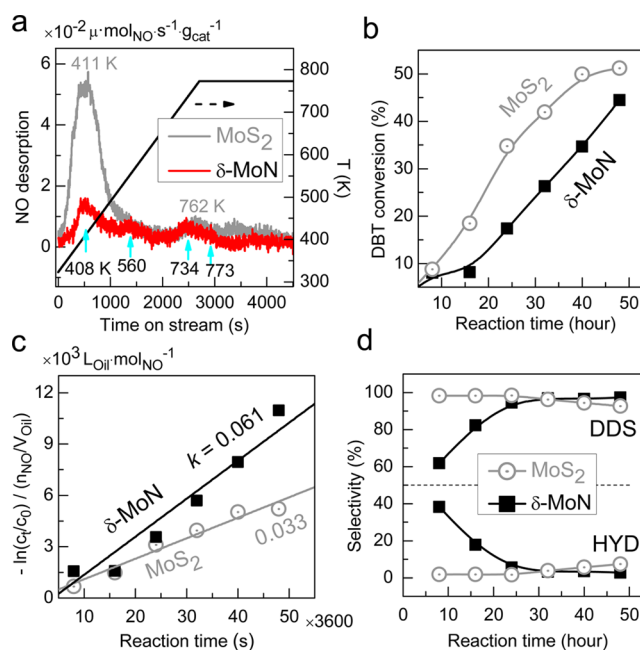

Figure 4. Catalytic activities of onion-like δ-MoN in the hydrodesulfurization (HDS) of dibenzothiophene (DBT). Traditional catalyst MoS_2 was also tested for comparison. (a) Temperature-programmed desorption (TPD) of NO gas molecules to determine the number of active Mo sites in each catalyst, which was pre-exposed to NO gas at 323 K for 60 min to absorb NO molecules and form Mo−NO bonds with unsaturated active Mo sites. (b) HDS of DBT at 623 K and 6 MPa in a H_2 atmosphere. (c) Relative DBT concentration, c_t/c_0, as a function of reaction time t. The pseudo-first-order rate constant, k, was deduced by linear fits of the plotted data. (d) Measured selectivity of direct desulfurization (DDS) and hydrogenation (HYD) in the HDS of DBT. The reaction detail for both DDS and HYD refers to ref30.

have different spectrum profiles probably due to their structural difference (see more detail in Supporting Information, Figure S5).

For layer-structured MoS_2, the desorption spectrum is characterized by a main peak at 411 K and a weaker satellite peak at a higher temperature of 762 K, which is theoretically attributed to coordinately unsaturated $(10\bar{1}0)$ and $(\bar{1}010)$ Mo sites on the edge of hexagonally packed slabs.[18] Similar desorption lines have also been observed in 3R-MoN_2,[30] a newly discovered nitrogen-rich nitride with a layered structure. Intriguingly, the onion-like MoN sample shows four distinct desorption peaks at 408, 560, 734, and 773 K (Figure 4a), indicating complicated sorption modes of the (101) "onion" surface with NO molecules. Continuing the argument along this line, the surface N atoms of this nitride may also be active, in addition to metal atoms, for adsorbing some special molecules (such as the −NO_2 group in ref 22), which would lead to more selective catalysis. By analysis of the NO uptake data, the molar volume for the absorbed NO can be quantified, and they are listed in Table 2 (also see Supporting Information,

Figure S5). The obtained ratio between δ-MoN and MoS$_2$ is NO$_{\delta\text{-MoN}}$:NO$_{\text{MoS2}}$ = 0.39:1, which is used in this work to normalize catalytic activity between the two catalysts. Accordingly, the concentration of catalytically active Mo centers can also be estimated using the NO/Mo ratio as listed in Table 2. It is worthwhile to point out that the attempt to perform CO uptake test with δ-MoN catalyst was unsuccessful, likely because of the weak adsorption interaction with CO molecules. Future theoretical work is warranted to fully explore the adsorption behaviors of onion-like δ-MoN with both NO and CO molecules.

The comparative results of HDS of DBT using both δ-MoN and MoS$_2$ catalysts are shown in Figure 4b and the catalytic reaction proceeded at 623 K. As expected from the surface area determination (Table 2), the DBT conversion using δ-MoN is lower than using traditional MoS$_2$ catalyst at the early stage of HDS. Overall, after 2 days of the reaction, $\sim$ 45% DBT conversion was achieved using δ-MoN, close to that using MoS$_2$ ($\sim$50%). The catalytic activity can be described by a pseudo-first-order rate constant, k, for the HDS of DBT, given by

$$\ln \frac{C_t}{C_0} = -\frac{k(n_{\text{NO}})}{V_{\text{Oil}}}t \qquad (2)$$

where c_t/c_0 denotes the ratio of DBT concentration between reaction time t and $t = 0$, V_{Oil} is the volume of the feed solution (i.e.,101.1 mL DBT and decalin oil), and n_{NO} represents the number of active Mo sites. On the basis of NO uptake data in Table 2, the determined ratio for the active Mo sites between δ-MoN and MoS$_2$ is 0.39:1, which is employed to determine the k value. Such-obtained k values for MoN and MoS$_2$ are 0.061 and 0.033 L$_{\text{Oil}}\cdot$(mol$_{\text{NO}}$)$^{-1}\cdot$s^{-1}, respectively. Apparently, δ-MoN is nearly twice more active than the traditional MoS$_2$ catalyst, presumably due to the onion-like structure of δ-MoN with highly exposed (101) crystallographic plane (see Figure 2 and Supporting Information, Figure S3).

Also plotted in Figure 4d is the reaction selectivity for both catalysts. Compared with MoS$_2$, δ-MoN catalyst is approximately 20 times more active for the hydrogenation (HYD) of DBT at the early reaction stage (refer to ref 30 for the detailed reaction for both HYD and DDS), and even more so compared to commercial catalysts such as Ni−MoS$_2$/Al$_2$O$_3$.[67] However, as the reaction proceeds, the selective activity of HYD for δ-MoN progressively deteriorates and eventually levels off at a similar value to that of MoS$_2$ after 30 h (Figure 4d). One plausible explanation is that the dissociation of reaction products from the surface of the nitride catalyst is impeded due to strong adsorption modes associated with nitrogen atoms. Hence, further optimization of catalytic properties of δ-MoN is needed to extrinsically improve its selectivity. Nevertheless, the results presented in this work demonstrate that the onion-like δ-MoN catalyst has excellent intrinsic activities for hydrogenation processes and is highly attractive from the perspectives of ultra-deep hydrodesulfurization of fossil fuels.[1]
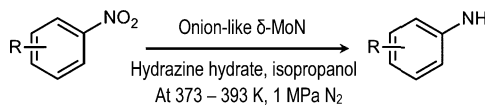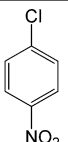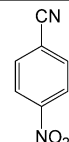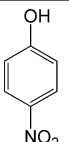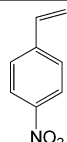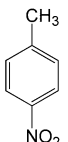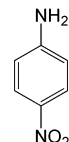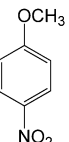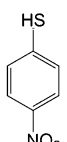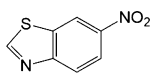
The catalytic activities were also evaluated using onion-like δ-MoN as a catalyst in the selective hydrogenation of nitroarenes to the corresponding anilines, the latter of which are key intermediates in the fine chemical, agrochemical, and pharmaceutical industries.[2,4,22] Because of the presence of other easily reducible groups in nitroarenes, certain catalysis are required to selectively hydrogenate only the nitro group (i.e.,

−NO$_2$) in functionalized substrates. Over the past few decades, for the production of anilines, the traditional Béchamp process has largely been replaced by environmentally more benign protocols involving noble metal catalysts (such as Pt, Au, and Pd).[2,68,69] However, these catalysts are not cost-effective because of their limited supply, which has spurred much interest in the search for inexpensive, base metal catalysts. The discovery of nitrogen-doped A$_x$O (A = Fe and Co) catalysts made of earth-abundant elements represents a great success.[4,22] More importantly, the incorporated nitrogen atoms in these catalysts play a key role in the selective adsorption of nitro group and selective hydrogenation when working cooperatively with metal atoms.[4,22]

Inspired by these recent developments, TM nitrides are expected to be promising catalysts with enhanced selectivity and activity, closely associated with N and metal atoms, respectively. Thus, we assessed the catalytic properties of onion-like δ-MoN as a catalyst for selective hydrogenation of nitroarenes. To obviate the need for autoclaves and high H$_2$ pressure,[4,22] hydrazine hydrate, N$_2$H$_4\cdot$H$_2$O, was used as reducing agent. As a hydrogen source, hydrazine hydrate has frequently been used in selective hydrogenation of nitro compounds.[70] The 2-propanol is served as a solvent, which is relatively non-toxic and dissolves a wide range of nonpolar compounds, compared to alternative solvents. In this work, the catalytic reaction proceeds in a liquid medium under industrially viable conditions of 373−393 K and 1 MPa N$_2$ atmosphere.

Our preliminary results are listed in Table 3. A typical example of phase identification and analysis of the final product can be found in Supporting Information, Figure S7. The

Table 3. Catalytic Hydrogenation of a Number of Substituted Nitroarenes to the Corresponding Anilines Using the Onion-Like δ-MoN Catalyst[a]

[a]Hydrazine hydrate is used as a reducing agent with 2-propanol as a solvent. Key: (a) The percentages represent the yield of aniline and are calculated from percentages of both conversion and selectivity. (b) The catalytic reaction proceeds for 8−24 h to maximize the yield.

catalytic hydrogenation using the δ-MoN catalyst is demonstrated in the reduction of more than 10 substituted nitro compounds with either electron-withdrawing (e.g., halogen, carbonyl, and nitril) or electron-releasing groups (e.g., alkyl, alcohol, and amino). A number of industrially important anilines are produced in excellent yields such as chloroaniline in Table 3, entry 1. Notably, the selective reduction of $-NO_2$ group in the presence of other reducible, functional substituents, such as alkene ($-C=C$) and hydroxyl ($-OH$), a challenging process for most traditional catalysts, is also achieved with good to excellent yields (i.e., 84.2−100%) (see Table 3, entries 3 and 4). It is noted that the product yield for certain anilines (e.g., entry 10 in Table 3) in this work is higher than the case using other earth-abundant metal compound catalysts with high pressure H_2 as a hydrogen source, such as N-doped AO_x (A = Fe and Co),[4,22] suggesting superior catalytic activity of this nitride catalyst. As an important transformation in organic chemistry, the reduction of functionalized nitrobenzene with cyano ($-C\equiv N$) group over the nitride catalyst gives a full conversion of 4-cyanoaniline (Table 3, entry 2). The nitride catalyst is also able to selectively synthesize amino heterocycle in excellent yield from the corresponding nitroarene (Table 3, entry 10). Furthermore, it can tolerate the substrate containing carboxylic ($-COOH$) group (Table 3, entry 9). Interestingly, sulfur-bearing anilines can also be produced from selective hydrogenation of the associated nitro compounds (Table 3, entries 8 and 10) without any detectable concurrent reduction of sulfur group, indicating a different reaction process from the hydrodefurization as discussed above. Clearly, the N and Mo atoms in the nitride catalyst work synergistically for more preferable adsorption of $-NO_2$ on the N sites, followed by hydrogenation of catalytically active Mo centers. Coupled with high stability and recyclability, the as-synthesized δ-MoN is an intrinsically superior catalyst for selective hydrogenation processes with tolerance to a broad range of functional groups.

To date, preparation of nanocrystals with onion-like morphology is primarily limited to material systems with layered structures as discussed above.[60−64] δ-MoN is in this regard the first non-layered metal nitride that has successfully been fabricated with an onion-like morphology at the nanoscale. Owing to the peculiar atomic arrangement of onion-like structure, the nitride catalyst exhibits superior catalytic activities for the HDS of DBT and selective hydrogenation of nitroaromatics to the corresponding anilines. Considering the cost and environmental advantages, this base-metal nitride catalyst holds great promise for the next-generation catalysts for a wide range of applications. Conceivably, the discovery of onion-like δ-MoN may open new opportunities for developments of highly active, MoN-based catalysts through introduction of promoter species (e.g., Co and Ni) and supporting substrates (e.g., Al_2O_3 and SiO_2), as already demonstrated for traditional catalysts.[1,15] We also expect that our findings will stimulate further research interest in the high-P fabrication of onion-like nanostructured catalysts in other hexagonal, refractory metal nitride systems (such as GaN,[58,59] WN,[40] and W_2N_3[40]) for enhanced catalytic performance.

CONCLUSIONS

In summary, we have successfully fabricated an onion-like, nanostructured δ-MoN catalyst with controllable grain size, using a high-P synthesis methodology. The concentrically-assembled onion shells of δ-MoN are made of bended (101) lattice planes having a peculiar zigzag Mo−N bonding structure. Most importantly, the as-synthesized δ-MoN exhibits superior catalytic activities and high hydrogenation selectivity over MoS_2 in the hydrodesulfurization of dibenzothiophene. In addition, the onion-like catalyst is catalytically favorable for selective hydrogenation of functionalized nitroarenes to the corresponding anilines with good to excellent yields and high tolerance to other functional groups including sensitive substituents (e.g., ketone, alkene, and hydroxyl). The excellent catalytic performances of this nitride catalyst are presumably attributed to a synergistic effect between Mo and N atoms on the zigzag onion surface. The nitride catalyst can be fabricated at moderate pressures of 3−5 GPa, making it feasible for massive and industrial-scale production.

ASSOCIATED CONTENT

Ⓢ Supporting Information

The Supporting Information is available free of charge on the ACS Publications website at DOI: 10.1021/acs.jpcc.7b05460.

> More detailed sample characterizations such as NPD, XRD, TEM, and temperature-programmed desorption (TPD) analysis (PDF)

AUTHOR INFORMATION

Corresponding Authors
*E-mail: wangsm@sustc.edu.cn (S.W.).
*E-mail: gehui@sxicc.ac.cn (H.G.).
*E-mail: zhaoys@sustc.edu.cn (Y.Z.).

ORCID Ⓞ
Shanmin Wang: 0000-0001-7273-2786
Hui Ge: 0000-0002-7486-8799
Zewei Quan: 0000-0003-1998-5527
Xiaodong Wen: 0000-0001-5626-8581

Notes
The authors declare no competing financial interest.

REFERENCES

(1) Song, C. An Overview of New Approaches to Deep Desulfurization for Ultra-Clean Gasoline, Diesel Fuel and Jet Fuel. *Catal. Today* **2003**, *86*, 211−263.

(2) Blaser, H.-U.; Steiner, H.; Studer, M. Selective Catalytic Hydrogenation of Functionalized Nitroarenes: An Update. *ChemCatChem* **2009**, *1*, 210−221.

(3) Ruditskiy, A.; Peng, H.-C.; Xia, Y. Shape-Controlled Metal Nanocrystals for Heterogeneous Catalysis. *Annu. Rev. Chem. Biomol. Eng.* **2016**, *7*, 327−348.

(4) Westerhaus, F. A.; Jagadeesh, R. V.; Wienhöfer, G.; Pohl, M.-M.; Radnik, J.; Surkus, A.-E.; Rabeah, J.; Junge, K.; Junge, H.; Nielsen, M.; et al. Heterogenized Cobalt Oxide Catalysts for Nitroarene Reduction

by Pyrolysis of Molecularly Defined Complexes. *Nat. Chem.* **2013**, *5*, 537−543.

(5) Farnetti, E.; Monte, D. R.; Kaspar, J. *Homogeneous and Heterogeneous Catalysis*; Eolss Publishers: Oxford, U.K., 2009; Vol. *II*, p 502.

(6) Norskov, J. K.; Bligaard, T.; Rossmeisl, J.; Christensen, C. H. Towards the Computational Design of Solid Catalysts. *Nat. Chem.* **2009**, *1*, 37−46.

(7) Mavrikakis, M.; Hammer, B.; Nørskov, J. K. Effect of Strain on the Reactivity of Metal Surfaces. *Phys. Rev. Lett.* **1998**, *81*, 2819−2822.

(8) Lee, I.; Morales, R.; Albiter, M. A.; Zaera, F. Synthesis of Heterogeneous Catalysts with Well Shaped Platinum Particles to Control Reaction Selectivity. *Proc. Natl. Acad. Sci. U. S. A.* **2008**, *105*, 15241−15246.

(9) Wei, H.; Liu, X.; Wang, A.; Zhang, L.; Qiao, B.; Yang, X.; Huang, Y.; Miao, S.; Liu, J.; Zhang, T. Feox-Supported Platinum Single-Atom and Pseudo-Single-Atom Catalysts for Chemoselective Hydrogenation of Functionalized Nitroarenes. *Nat. Commun.* **2014**, *5*, 5634.

(10) Tian, N.; Zhou, Z.-Y.; Yu, N.-F.; Wang, L.-Y.; Sun, S.-G. Direct Electrodeposition of Tetrahexahedral Pd Nanocrystals with High-Index Facets and High Catalytic Activity for Ethanol Electrooxidation. *J. Am. Chem. Soc.* **2010**, *132*, 7580−7581.

(11) Cao, S.; Tao, F.; Tang, Y.; Li, Y.; Yu, J. Size- and Shape-Dependent Catalytic Performances of Oxidation and Reduction Reactions on Nanocatalysts. *Chem. Soc. Rev.* **2016**, *45*, 4747−4765.

(12) Porter, N. S.; Wu, H.; Quan, Z.; Fang, J. Shape-Control and Electrocatalytic Activity-Enhancement of Pt-Based Bimetallic Nanocrystals. *Acc. Chem. Res.* **2013**, *46*, 1867−1877.

(13) Sealy, C. The Problem with Platinum. *Mater. Today* **2008**, *11*, 65−68.

(14) Bullock, R. M. Abundant Metals Give Precious Hydrogenation Performance. *Science* **2013**, *342*, 1054−1055.

(15) Anand, M.; Sughrue, E. L.; Yao, J. *Mos2 Catalyst for the Conversion of Sugar Alcohol to Hydrocarbons*. Patent: US 2012/0215047A1, 2012.

(16) Voiry, D.; Yamaguchi, H.; Li, J.; Silva, R.; Alves, D. C. B.; Fujita, T.; Chen, M.; Asefa, T.; Shenoy, V. B.; Eda, G.; et al. Enhanced Catalytic Activity in Strained Chemically Exfoliated Ws2 Nanosheets for Hydrogen Evolution. *Nat. Mater.* **2013**, *12*, 850−855.

(17) Bernardi, M.; Palummo, M.; Grossman, J. C. Extraordinary Sunlight Absorption and One Nanometer Thick Photovoltaics Using Two-Dimensional Monolayer Materials. *Nano Lett.* **2013**, *13*, 3664−3670.

(18) Zeng, T.; Wen, X.-D.; Li, Y.-W.; Jiao, H. Density Functional Theory Study of Triangular Molybdenum Sulfide Nanocluster and Co Adsorption on It. *J. Phys. Chem. B* **2005**, *109*, 13704−13710.

(19) Jaramillo, T. F.; Jørgensen, K. P.; Bonde, J.; Nielsen, J. H.; Horch, S.; Chorkendorff, I. Identification of Active Edge Sites for Electrochemical H2 Evolution from Mos2 Nanocatalysts. *Science* **2007**, *317*, 100−102.

(20) Somorjai, G. A.; Rupprechter, G. Molecular Studies of Catalytic Reactions on Crystal Surfaces at High Pressures and High Temperatures by Infrared−Visible Sum Frequency Generation (Sfg) Surface Vibrational Spectroscopy. *J. Phys. Chem. B* **1999**, *103*, 1623−1638.

(21) Stamenkovic, V. R.; Fowler, B.; Mun, B. S.; Wang, G.; Ross, P. N.; Lucas, C. A.; Marković, N. M. Improved Oxygen Reduction Activity on Pt3ni(111) Via Increased Surface Site Availability. *Science* **2007**, *315*, 493−497.

(22) Jagadeesh, R. V.; Surkus, A.-E.; Junge, H.; Pohl, M.-M.; Radnik, J.; Rabeah, J.; Huan, H.; Schünemann, V.; Brückner, A.; Beller, M. Nanoscale Fe2o3-Based Catalysts for Selective Hydrogenation of Nitroarenes to Anilines. *Science* **2013**, *342*, 1073−1076.

(23) Abe, H.; Cheung, T. K.; Bell, A. T. The Activity of Transition Metal Nitrides for Hydrotreating Quinoline and Thiophene. *Catal. Lett.* **1993**, *21*, 11−18.

(24) Wang, D.; Zhu, Y.; Tian, C.; Wang, L.; Zhou, W.; Dong, Y.; Han, Q.; Liu, Y.; Yuan, F.; Fu, H. Synergistic Effect of Mo2n and Pt for Promoted Selective Hydrogenation of Cinnamaldehyde over Pt-Mo2n/Sba-15. *Catal. Sci. Technol.* **2016**, *6*, 2403−2412.

(25) Wyvratt, B. M.; Gaudet, J. R.; Pardue, D. B.; Marton, A.; Rudić, S.; Mader, E. A.; Cundari, T. R.; Mayer, J. M.; Thompson, L. T. Reactivity of Hydrogen on and in Nanostructured Molybdenum Nitride: Crotonaldehyde Hydrogenation. *ACS Catal.* **2016**, *6*, 5797−5806.

(26) Neylon, M. K.; Choi, S.; Kwon, H.; Curry, K. E.; Thompson, L. T. Catalytic Properties of Early Transition Metal Nitrides and Carbides: N-Butane Hydrogenolysis, Dehydrogenation and Isomerization. *Appl. Catal., A* **1999**, *183*, 253−263.

(27) Tabata, M.; Maeda, K.; Higashi, M.; Lu, D.; Takata, T.; Abe, R.; Domen, K. Modified Ta3n5 Powder as a Photocatalyst for O2 Evolution in a Two-Step Water Splitting System with an Iodate/Iodide Shuttle Redox Mediator under Visible Light. *Langmuir* **2010**, *26*, 9161−9165.

(28) Chen, W.-F.; Muckerman, J. T.; Fujita, E. Recent Developments in Transition Metal Carbides and Nitrides as Hydrogen Evolution Electrocatalysts. *Chem. Commun.* **2013**, *49*, 8896−8909.

(29) Zhao, Y.; Kamiya, K.; Hashimoto, K.; Nakanishi, S. In Situ Co2-Emission Assisted Synthesis of Molybdenum Carbonitride Nanomaterial as Hydrogen Evolution Electrocatalyst. *J. Am. Chem. Soc.* **2015**, *137*, 110−113.

(30) Wang, S.; Ge, H.; Sun, S.; Zhang, J.; Liu, F.; Wen, X.; Yu, X.; Wang, L.; Zhang, Y.; Xu, H.; et al. A New Molybdenum Nitride Catalyst with Rhombohedral Mos2 Structure for Hydrogenation Applications. *J. Am. Chem. Soc.* **2015**, *137*, 4815−4822.

(31) Cao, B.; Veith, G. M.; Neuefeind, J. C.; Adzic, R. R.; Khalifah, P. G. Mixed Close-Packed Cobalt Molybdenum Nitrides as Non-Noble Metal Electrocatalysts for the Hydrogen Evolution Reaction. *J. Am. Chem. Soc.* **2013**, *135*, 19186−19192.

(32) Zerr, A.; Miehe, G.; Riedel, R. Synthesis of Cubic Zirconium and Hafnium Nitride Having Th3p4 Structure. *Nat. Mater.* **2003**, *2*, 185−189.

(33) Salamat, A.; Hector, A. L.; Gray, B. M.; Kimber, S. A. J.; Bouvier, P.; McMillan, P. F. Synthesis of Tetragonal and Orthorhombic Polymorphs of Hf3n4 by High-Pressure Annealing of a Prestructured Nanocrystalline Precursor. *J. Am. Chem. Soc.* **2013**, *135*, 9503−9511.

(34) Zerr, A.; Miehe, G.; Li, J.; Dzivenko, D. A.; Bulatov, V. K.; Hoefer, H.; Bolfan-Casanova, N.; Fialin, M.; Brey, G.; Watanabe, T.; et al. High-Pressure Synthesis of Tantalum Nitride Having Orthorhombic U2s3 Type Structure. *Adv. Funct. Mater.* **2009**, *19*, 2282−2288.

(35) Salamat, A.; Woodhead, K.; Shah, S. I. U.; Hector, A. L.; McMillan, P. F. Synthesis of U3se5 and U3te5 Type Polymorphs of Ta3n5 by Combining High Pressure-Temperature Pathways with a Chemical Precursor Approach. *Chem. Commun.* **2014**, *50*, 10041−10044.

(36) Gregoryanz, E.; Sanloup, C.; Somayazulu, M.; Badro, J.; Fiquet, G.; Mao, H. K.; Hemley, R. J. Synthesis and Characterization of a Binary Noble Metal Nitride. *Nat. Mater.* **2004**, *3*, 294−297.

(37) Young, A. F.; Sanloup, C.; Gregoryanz, E.; Scandolo, S.; Hemley, R. J.; Mao, H.-k. Synthesis of Novel Transition Metal Nitrides Irn2 and Osn2. *Phys. Rev. Lett.* **2006**, *96*, 155501.

(38) Friedrich, A.; Winkler, B.; Bayarjargal, L.; Morgenroth, W.; Juarez-Arellano, E. A.; Milman, V.; Refson, K.; Kunz, M.; Chen, K. Novel Rhenium Nitrides. *Phys. Rev. Lett.* **2010**, *105*, 085504.

(39) Crowhurst, J. C.; Goncharov, A. F.; Sadigh, B.; Evans, C. L.; Morrall, P. G.; Ferreira, J. L.; Nelson, A. J. Synthesis and Characterization of the Nitrides of Platinum and Iridium. *Science* **2006**, *311*, 1275−1278.

(40) Wang, S.; Yu, X.; Lin, Z.; Zhang, R.; He, D.; Qin, J.; Zhu, J.; Han, J.; Wang, L.; Mao, H.-K.; et al. Synthesis, Crystal Structure, and Elastic Properties of Novel Tungsten Nitrides. *Chem. Mater.* **2012**, *24*, 3023−3028.

(41) Chen, M.; Wang, S.; Zhang, J.; He, D.; Zhao, Y. Synthesis of Stoichiometric and Bulk Crn through a Solid-State Ion-Exchange Reaction. *Chem. - Eur. J.* **2012**, *18*, 15459−15463.

(42) Wang, S.; Yu, X.; Zhang, J.; Chen, M.; Zhu, J.; Wang, L.; He, D.; Lin, Z.; Zhang, R.; Leinenweber, K.; et al. Experimental Invalidation of

Phase-Transition-Induced Elastic Softening in Crn. *Phys. Rev. B: Condens. Matter Mater. Phys.* **2012**, *86*, 064111.

(43) Wu, F.; Huang, C.; Wu, H.; Lee, C.; Deng, K.; Kan, E.; Jena, P. Atomically Thin Transition-Metal Dinitrides: High-Temperature Ferromagnetism and Half-Metallicity. *Nano Lett.* **2015**, *15*, 8277−8281.

(44) Wang, Y.; Wang, S.-S.; Lu, Y.; Jiang, J.; Yang, S. A. Strain-Induced Isostructural and Magnetic Phase Transitions in Monolayer Mon₂. *Nano Lett.* **2016**, *16*, 4576−4582.

(45) Wang, S.; Yu, X.; Zhang, J.; Wang, L.; Leinenweber, K.; He, D.; Zhao, Y. Synthesis, Hardness, and Electronic Properties of Stoichiometric Vn and Crn. *Cryst. Growth Des.* **2016**, *16*, 351−358.

(46) Wang, S.; Antonio, D.; Yu, X.; Zhang, J.; Cornelius, A. L.; He, D.; Zhao, Y. The Hardest Superconducting Metal Nitride. *Sci. Rep.* **2015**, *5*, 13733.

(47) Wang, S.; He, D.; Wang, W.; Lei, L. Pressure Calibration for the Cubic Press by Differential Thermal Analysis and the High-Pressure Fusion Curve of Aluminum. *High Pressure Res.* **2009**, *29*, 806−814.

(48) Brunauer, S.; Emmett, P. H.; Teller, E. Adsorption of Gases in Multimolecular Layers. *J. Am. Chem. Soc.* **1938**, *60*, 309−319.

(49) Ganin, A. Y.; Kienle, L.; Vajenine, G. V. Synthesis and Characterisation of Hexagonal Molybdenum Nitrides. *J. Solid State Chem.* **2006**, *179*, 2339−2348.

(50) Cao, B.; Neuefeind, J. C.; Adzic, R. R.; Khalifah, P. G. Molybdenum Nitrides as Oxygen Reduction Reaction Catalysts: Structural and Electrochemical Studies. *Inorg. Chem.* **2015**, *54*, 2128−2136.

(51) Bull, C. L.; McMillan, P. F.; Soignard, E.; Leinenweber, K. Determination of the Crystal Structure of Δ-Mon by Neutron Diffraction. *J. Solid State Chem.* **2004**, *177*, 1488−1492.

(52) Sears, V. F. Neutron Scattering Lengths and Cross Sections. *Neutron News* **1992**, *3*, 26−37.

(53) Zhang, Y.; Haberkorn, N.; Ronning, F.; Wang, H.; Mara, N. A.; Zhuo, M.; Chen, L.; Lee, J. H.; Blackmore, K. J.; Bauer, E.; et al. Epitaxial Superconducting Δ-Mon Films Grown by a Chemical Solution Method. *J. Am. Chem. Soc.* **2011**, *133*, 20735−20737.

(54) Kazmanli, M. K.; Ürgen, M.; Cakir, A. F. Effect of Nitrogen Pressure, Bias Voltage and Substrate Temperature on the Phase Structure of Mo−N Coatings Produced by Cathodic Arc Pvd. *Surf. Coat. Technol.* **2003**, *167*, 77−82.

(55) Chen, W.-F.; Sasaki, K.; Ma, C.; Frenkel, A. I.; Marinkovic, N.; Muckerman, J. T.; Zhu, Y.; Adzic, R. R. Hydrogen-Evolution Catalysts Based on Non-Noble Metal Nickel−Molybdenum Nitride Nanosheets. *Angew. Chem., Int. Ed.* **2012**, *51*, 6131−6135.

(56) Inumaru, K.; Nishikawa, T.; Nakamura, K.; Yamanaka, S. High-Pressure Synthesis of Superconducting Molybdenum Nitride Δ-Mon by in Situ Nitridation. *Chem. Mater.* **2008**, *20*, 4756−4761.

(57) Zhao, X. D.; Range, K. J. High Pressure Synthesis of Molybdenum Nitride Mon. *J. Alloys Compd.* **2000**, *296*, 72−74.

(58) Ma, H.; He, D.; Lei, L.; Wang, S.; Chen, Y.; Wang, H. Gan Crystals Prepared through Solid-State Metathesis Reaction from Nagao₂ and Bn under High Pressure and High Temperature. *J. Alloys Compd.* **2011**, *509*, L124−L127.

(59) Lei, L.; He, D. Synthesis of Gan Crystals through Solid-State Metathesis Reaction under High Pressure. *Cryst. Growth Des.* **2009**, *9*, 1264−1266.

(60) Tian, Y.; Xu, B.; Yu, D.; Ma, Y.; Wang, Y.; Jiang, Y.; Hu, W.; Tang, C.; Gao, Y.; Luo, K.; et al. Ultrahard Nanotwinned Cubic Boron Nitride. *Nature* **2013**, *493*, 385−388.

(61) Tenne, R. Inorganic Nanotubes and Fullerene-Like Nanoparticles. *Nat. Nanotechnol.* **2006**, *1*, 103−111.

(62) Kuznetsov, V. L.; Chuvilin, A. L.; Butenko, Y. V.; Mal'kov, I. Y.; Titov, V. M. Onion-Like Carbon from Ultra-Disperse Diamond. *Chem. Phys. Lett.* **1994**, *222*, 343−348.

(63) Huang, Q.; Yu, D.; Xu, B.; Hu, W.; Ma, Y.; Wang, Y.; Zhao, Z.; Wen, B.; He, J.; Liu, Z.; et al. Nanotwinned Diamond with Unprecedented Hardness and Stability. *Nature* **2014**, *510*, 250−253.

(64) Guo, Q.; Yang, Q.; Yi, C.; Zhu, L.; Xie, Y. Synthesis of Carbon Nitrides with Graphite-Like or Onion-Like Lamellar Structures Via a Solvent-Free Route at Low Temperatures. *Carbon* **2005**, *43*, 1386−1391.

(65) Miao, B.-T.; Wang, S.-M.; Kong, P.-P.; Jin, M.-L.; Feng, S.-M.; Zhang, S.-J.; Hao, A.-M.; Yu, X.-H.; Jin, C.-Q.; Zhao, Y.-S. Effects of Pressure and/or Magnetism on Superconductivity of Δ-Mon Single Crystal. *Chin. Phys. B* **2015**, *24*, 017403.

(66) Valencia, D.; Klimova, T. Citric Acid Loading for Mos₂-Based Catalysts Supported on Sba-15. New Catalytic Materials with High Hydrogenolysis Ability in Hydrodesulfurization. *Appl. Catal., B* **2013**, *129*, 137−145.

(67) Cho, A.; Lee, J. J.; Koh, J. H.; Wang, A.; Moon, S. H. Performance of Nimos/Al₂o₃ Prepared by Sonochemical and Chemical Vapor Deposition Methods in the Hydrodesulfurization of Dibenzothiophene and 4,6-Dimethyldibenzothiophene. *Green Chem.* **2007**, *9*, 620−625.

(68) Corma, A.; Serna, P. Chemoselective Hydrogenation of Nitro Compounds with Supported Gold Catalysts. *Science* **2006**, *313*, 332−334.

(69) Cai, S.; Duan, H.; Rong, H.; Wang, D.; Li, L.; He, W.; Li, Y. Highly Active and Selective Catalysis of Bimetallic Rh₃ni₁ Nanoparticles in the Hydrogenation of Nitroarenes. *ACS Catal.* **2013**, *3*, 608−612.

(70) Jagadeesh, R. V.; Wienhofer, G.; Westerhaus, F. A.; Surkus, A.-E.; Pohl, M.-M.; Junge, H.; Junge, K.; Beller, M. Efficient and Highly Selective Iron-Catalyzed Reduction of Nitroarenes. *Chem. Commun.* **2011**, *47*, 10972−10974.